Chemical Science

ROYAL SOCIETY OF CHEMISTRY

EDGE ARTICLE

View Article Online
View Journal | View Issue

Cite this: *Chem. Sci.*, 2020, **11**, 3371

All publication charges for this article have been paid for by the Royal Society of Chemistry

Received 16th January 2020
Accepted 25th February 2020

DOI: 10.1039/d0sc00290a

rsc.li/chemical-science

In vivo real-time tracking of tumor-specific biocatalysis in cascade nanotheranostics enables synergistic cancer treatment†

Ruofei Wang,‡ Chenxu Yan, ‡ Hehe Zhang, Zhiqian Guo * and Wei-Hong Zhu

Glucose oxidase (GOD)-based synergistic cancer therapy has aroused great research interest in the context of cancer treatment due to the inherent biocompatibility and biodegradability. However, this emerging therapeutic system still lacks a strategy to predict and regulate the *in vivo* biocatalytic behavior of GOD in real time to minimize the side effects on normal tissues. Herein, we developed a tumor-specific cascade nanotheranostic system (BNG) that combines GOD-catalyzed oxidative stress and dual-channel fluorescent sensing, significantly improving the synergistic therapeutic efficacy with real-time feedback information. The nanotheranostic system remains completely silent in the blood circulatory system and selectively releases GOD enzymes in the tumor site, with enhanced near-infrared (NIR) fluorescence at 825 nm. Subsequently, GOD catalyzes H_2O_2 production, triggering cascade reactions with NIR fluorescence at 650 nm as an optical output, along with GSH depletion, enabling synergistic cancer treatment. The designed nanotheranostic system, integrated with tumor-activated cascade reactions and triggering a dual-channel output at each step, represents an insightful paradigm for precise cooperative cancer therapy.

Introduction

The regulation of oxidative stress mediated by reactive oxygen species (ROS) has bloomed as an effective strategy for cancer treatment.[1–9] Particularly, the enzyme-catalyzed strategy that involves glucose oxidase (GOD) has received considerable attention because of its fascinating catalytic properties in depleting β-D-glucose with ROS generation, together with inherent biocompatibility and non-toxicity.[10–12] Most of the reported GOD-based biocatalytic strategies have mainly focused on the entrapment of GOD with tumor-specific nanocarriers for prolonged blood circulation duration, increased stability, and improved tumor-targeting ability.[13–21] Despite their significant advances, there remains a lack of desirable GOD-based design strategy to predict *in vivo* behaviors and regulate the therapeutic efficiency of GOD in clinical applications.

Abundant cellular glutathione (GSH) is well known to be capable of reducing oxidative stress; thus, developing functional nanosystems that can deplete the intracellular GSH level is beneficial for improving therapeutic efficiency.[22–27] It has been also proposed that the cascade process with GOD-catalyzed H_2O_2 generation followed by GSH depletion could finely regulate oxidative stress.[28–31] Thus, the integration of GSH scavengers with GOD-catalyzed H_2O_2 generation into a nanotheranostics system could effectively improve therapeutic efficiency.[32–38] However, for *in vivo* application, the elevated oxidative stress from this cascade system is a double-edged sword, inevitably leading to damage in normal tissues.[39] To date, owing to the dynamic nature of oxidative stress, it is still difficult to predict and regulate the *in vitro* and *in vivo* therapeutic effects of GOD-catalyzed cascade process. In this context, the combination of GOD-induced oxidative stress and optical imaging/sensing is expected to achieve synergistic therapeutic efficacy with real-time feedback information.

Herein, as a proof of concept for tracking tumor-specific biocatalysis in cascade nanotheranostics, we engineered GOD with a dual-channel near-infrared (NIR) molecular fluorescent probe coloaded into pH-sensitive copolymers. As illustrated in Fig. 1, this nanotheranostics system (named BNG) contains three components: GOD as a H_2O_2-generating catalyst, BP_5-Cy-B moiety as a dual-channel fluorescent signal reporter with phenylboronic ester for H_2O_2-specific recognition, and the diblock copolymers (N1) serving as container with ultrasensitive response to pH. First, BNG remains non-emissive at the normal pH of 7.4. When the nanoparticles are triggered and dissociate under pH < 6.8, both GOD and BP_5-Cy-B are together released, accompanied with turn-on

Key Laboratory for Advanced Materials, Joint International Research Laboratory of Precision Chemistry and Molecular Engineering, Feringa Nobel Prize Scientist Joint Research Center, Institute of Fine Chemicals, School of Chemistry and Molecular Engineering, East China University of Science and Technology, Shanghai 200237, China. E-mail: guozq@ecust.edu.cn

† Electronic supplementary information (ESI) available. See DOI: 10.1039/d0sc00290a

‡ These authors contributed equally to this work.

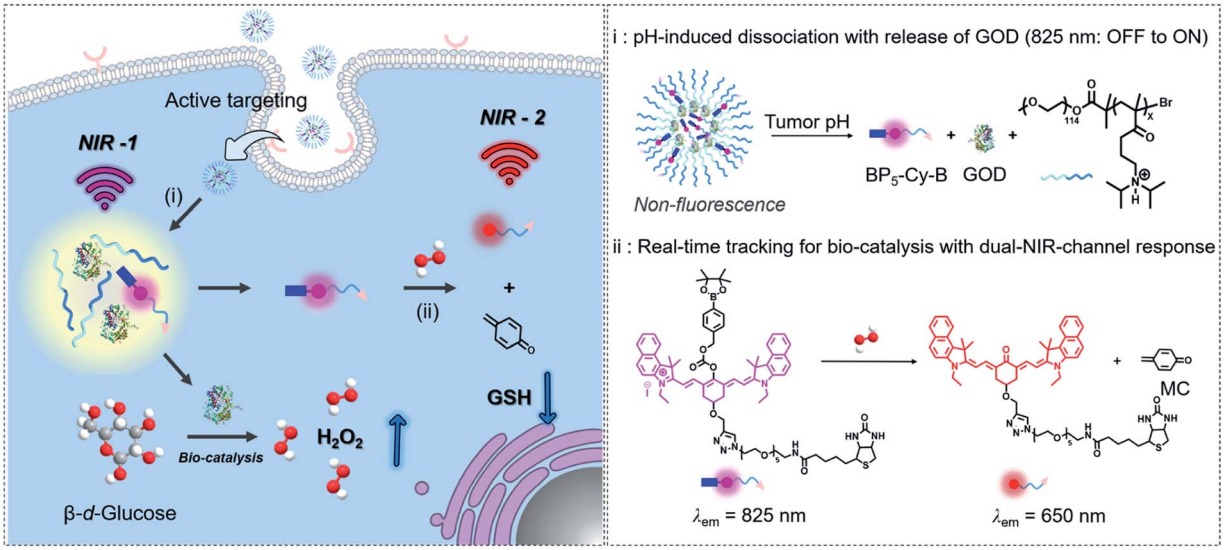

Fig. 1 Cascade tumor-specific nanotheranostics integrated with the *in vivo* real-time tracking of biocatalysis and synergistic treatment. Nanoparticle dissociation occurs in the acidic cellular microenvironment. Then, GOD and BP_5-Cy-B are released, along with turn-on emission at 825 nm (NIR-1). The released GOD effectively catalyzes the oxidation reaction of oxygen and glucose to produce large amounts of H_2O_2 and prevent tumor progress. The high concentration of H_2O_2 induces a dual-channel response (a remarkable shift from 825 to 650 nm, NIR-2) in BP_5-Cy-B with MC as by-products, which will suppress GSH levels to achieve synergistic tumor treatment.

emission at 825 nm (NIR-1, Fig. 1). Second, GOD catalyzes the reaction between oxygen and glucose, then produces a large amount of H_2O_2. Third, BP_5-Cy-B reacts with H_2O_2 generated by GOD, displaying a new emission band at 650 nm (NIR-2), and thus the byproduct quinone methide (MC) depletes intracellular GSH. Our strategy for cascade nanotheranostics integrates the following cooperative functions: (i) real-time *in vivo* tracking of GOD release; (ii) providing feedback on oxidative stress; and (iii) synergistically improved cancer treatment. The experimental results prove that the orchestrated nanotheranostics could be implemented for tracking the biocatalysis behaviors of GOD in living animals.

Results and discussion

Construction of cascade nanotheranostics

To sense cellular oxidative stress and track the behaviors of GOD in real time, we designed a H_2O_2-activated dual-channel NIR probe (BP_5-Cy-B) with two distinct fluorescent emissions as output signals. The probe comprises a cyanine-derivative chromophore that could be modulated by changing the π-conjugated system as a NIR fluorescence reporter, a phenylboronic ester group as a triggering moiety for H_2O_2, and a hydrophilic PEG oligomer-bridged biotin segment as an active tumor-targeting unit.[40–45] Then, we chose a diblock copolymer (named N1) as a pH-activated nanocarrier, which is composed of a PEG unit and copolymerized diisopropylamino-functionalized methacrylate. Importantly, this block copolymer N1 not only maintains the intact GOD inside the nanoparticles in normal tissues, but also promises the efficient release of GOD at the acidic tumor site. All the detailed procedures and characterization of BP_5-Cy-B and N1 are shown in the ESI.†

As depicted in Fig. 2A, BNG was obtained *via* physical encapsulation. Specifically, a dimethyl sulfoxide (DMSO) solution of BP_5-Cy-B and N1 was added dropwise into the aqueous solution of GOD, followed by dialysis against water to remove DMSO. In addition, we also constructed BN (only encapsulating BP_5-Cy-B into N1) as a control. As shown in Fig. 2B, dynamic light scattering (DLS) measurement reveals that the hydrodynamic diameters of BNG and BN were *ca.* 210 nm and 154 nm, respectively. These nanosized diameters of BNG and BN with well-defined sizes make them suitable for tumor accumulation through an enhanced permeability and retention (EPR) effect. Notably, BNG is larger than BN, which further confirmed that GOD was loaded into the nanocarriers.

Ultrasensitive H^+-triggered GOD release with turn-on NIR fluorescence at 825 nm

First of all, we focused on whether BNG could sense the pH change between tumor cells (pH 5.0–7.0) and blood (pH 7.4). In fact, we found that BNG initially formed compact, self-assembled nanoparticles at pH 7.4, which maintained non-emissive fluorescent properties (Fig. 2C and D). BP_5-Cy-B showed the typical ACQ (aggregation-caused quenching) property (Fig. S1†), resulting in completely quenched fluorescence at the formation of compact BNG nanoparticles. When the pH value changed from 7.4 to 5.4, the hydrophobic block in the copolymer chain became protonated, thus leading to disassembly of the initial compact nanoparticles, with a dramatic turn-on NIR fluorescence at 825 nm due to the molecular state of BP_5-Cy-B. Thus, in the acidic tumor microenvironment, BNG could be efficiently activated and the strong NIR signal at 825 nm could be utilized for tracking of H^+-triggered GOD release.

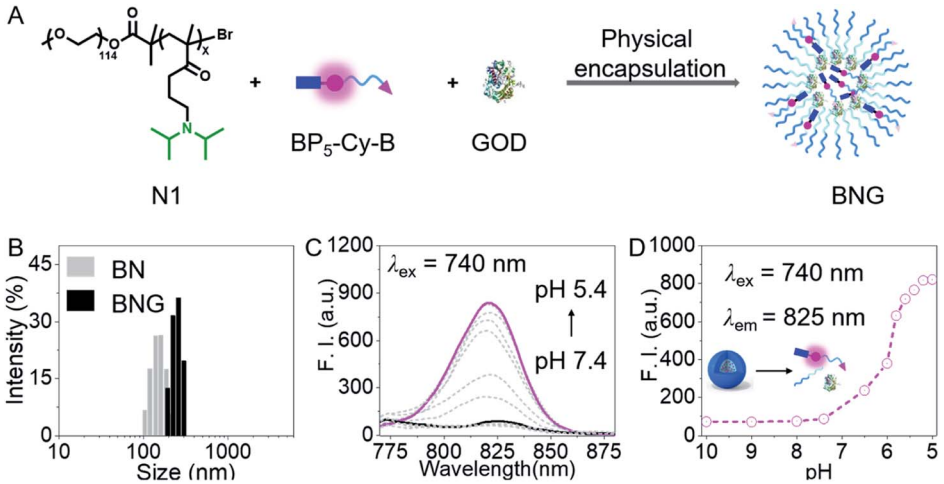

Fig. 2 The construction of the cascade nanotheranostics and ultrasensitive H^+-triggered GOD release with a turn-on signal at 825 nm. (A) The construction of BNG. (B) The size distribution (*via* dynamic light scattering analysis) of BN and BNG in aqueous solution at pH 7.4. (C and D) Fluorescence intensity as a function of pH for BNG. At a high pH (for example, 7.4), BNG remains silent. At a pH below 6.5, BNG is activated as a result of nanoparticle dissociation.

Tracking GOD-based cascade reaction process *via* dual-channel NIR fluorescence signal

To validate the feasibility of BNG for tracking the GOD-based cascade reaction driven by the two stimuli (pH and H_2O_2), we firstly assessed the dual-channel NIR fluorescence responses from the small probe BP_5-Cy-B. Upon the addition of H_2O_2, BP_5-Cy-B displayed a remarkable shift in the absorption spectra, along with the color change from green to purple-red. The absorption peak at 810 nm sharply decreased, and an increasing band centered at 540 nm was observed, along with a distinct isosbestic point at around 640 nm (Fig. 3B). Concomitantly, an obvious decrease in the emission spectra at 825 nm ($\lambda_{ex} = 740$ nm) and a sharp increase at 650 nm ($\lambda_{ex} = 540$ nm) were also observed in the emission spectra (Fig. 3C and D). These dual-channel switchable NIR responses could be attributed to the disruption in the polymethine π-electron system towards H_2O_2, resulting in a large hypsochromic shift in both the absorption and emission spectra. Impressively, this small probe BP_5-Cy-B possessed around 350-fold ratio enhancement ($I_{650\ nm}/I_{825\ nm}$) towards H_2O_2 over other potential reactive species (Fig. S2†), which indicated its excellent selectivity. All these results clearly demonstrated that the probe BP_5-Cy-B is capable of real-time monitoring of H_2O_2 concentrations *in vivo*, with remarkable dual-channel NIR responses.

We then investigated the utility of the aforementioned dual-channel fluorescence response for monitoring the GOD-based biocatalysis cascade reaction process. As is well known, GOD catalyzes the oxidation of glucose with high efficiency, producing H_2O_2. With this in mind, we directly incubated the probe BP_5-Cy-B (10 μM) with GOD (20 U mL^{-1}) and glucose (5 mg mL^{-1}) in solution. As expected, the dual-channel NIR fluorescence response in this mixed system was observed to be the same as the addition of H_2O_2 with the probe BP_5-Cy-B. That is, a NIR emission band at 825 nm obviously decreased, and concomitantly a new emission peak at 650 nm sharply increased (Fig. S3†). The sensing mechanism was further confirmed by ESI-MS (positive ion mode) analyses. The ionic peaks (m/z) of 1329.65 (corresponding to $[BP_5\text{-Cy-ph-OH}]^+$) and 1179.65 (corresponding to $[BP_5\text{-Cy-O} + H]^+$) were found in the high-resolution mass spectrum (Fig. S4†). It was demonstrated that there was a two-step process for the generation of the NIR reporter Cy-O (Scheme S3†): GOD is responsible for the

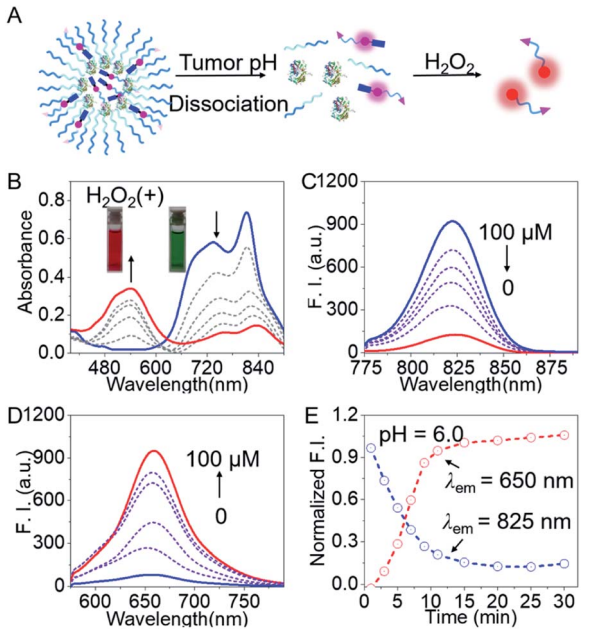

Fig. 3 Dual-channel response of cascade nanotheranostics triggered by two stimuli (pH and H_2O_2). (A) The cascade mechanism of BNG in a multistage tumor microenvironment. The absorption spectra (B) and fluorescence spectra ((C) $\lambda_{ex} = 740$ nm; (D) $\lambda_{ex} = 540$ nm) of the probe BP_5-Cy-B in the presence of H_2O_2 (DMSO/PBS, v/v = 1/3, pH = 7.4). (E) Normalized emission intensity ($\lambda_{em} = 825$ nm and $\lambda_{em} = 650$ nm) of BNG in the presence of H_2O_2 and pH at 6.0 for 30 min in aqueous solution.

generation of H_2O_2, and then the oxidization of the boronate moiety is triggered by H_2O_2, thus producing MC *via* elimination reaction. All these results strongly support the proposed sensing mechanism of BP_5-Cy-B with H_2O_2, and the desired capacity for real-time tracking of the GOD-based biocatalysis by the dual-channel switchable NIR fluorescence response.

Encouraged by the promising dual-channel NIR fluorescence response, BNG was elaborately designed and employed for tracking the GOD-based cascade reaction driven by pH and H_2O_2. As above mentioned, BNG could be efficiently activated under acidic condition (low pH) with a turn-on NIR emission signal at 825 nm. Specifically, the initial compact nanoparticles of BNG were disassembled at pH 6.0 with remarkable NIR emission at 825 nm in aqueous solution. Upon the addition of H_2O_2, BNG displayed an obvious blue shift from 825 nm to 650 nm in the emission spectra (Fig. 3E), and the emission intensity in this cascade system reached a plateau at around 15 min. Moreover, BNG nanoparticles kept their diameter and fluorescence intensity at 825 nm for over 80 h. These results indicate that BNG nanoparticles exhibit excellent and satisfactory stability for long-term storage (Fig. S5†). Thus, the dual-channel NIR response of BNG, driven by the two triggers (pH and H_2O_2), make it possible simultaneously to track where, when, and how GOD is released, along with its biocatalytic behavior.

Real-time monitoring of GOD-based cascade process in living cells

To investigate the ability of BNG to track the pH and H_2O_2 induced cascade reaction, we firstly verified the dual-channel responses of the probe BP_5-Cy-B in living cells. To investigate the *in vitro* cytotoxicity, we chose A549 cancer cells as the cell line model. In fact, BP_5-Cy-B exhibited almost no cytotoxic effects on cells, showing good biocompatibility. As shown in Fig. 4A, after the incubation of BP_5-Cy-B with A549 cancer cells, both of the fluorescence signals at 650 nm (red channel) and 825 nm (purple channel) were observed. This indicated that BP_5-Cy-B is activated by the endogenous H_2O_2 of A549 cells. Then, we further incubated A549 cells with exogenous H_2O_2, PMA (ROS trigger), or TEMPO (ROS scavenger). As expected, all these fluorescence intensities at 650 nm are consistent with their cellular H_2O_2 levels (Fig. 4B–D). Furthermore, compared with Cy-B (without biotin unit), BP_5-Cy-B displayed excellent cancer cell-targeting ability and mitochondria-targeting ability (Fig. 4D, E and S6, S7†). This could be attributed to the active targeting biotin unit of BP_5-Cy-B and its positive charge.[46,47] All these results confirmed that BP_5-Cy-B with dual-channel fluorescence response could be employed to detect different H_2O_2 levels in living cells and increase the targeting ability of BNG.

Considering the GOD-catalyzed oxidation of glucose with high efficiency to produce H_2O_2, the remarkable dual-channel fluorescence response of BP_5-Cy-B makes it possible to employ BNG for monitoring the GOD-based cascade process in living cells. This can be done by directly visualizing the release of GOD *via* a light-up emission at 825 nm, and real-time tracking the cascade catalytic reaction process *via* a new emission band at 650 nm with a significant shift. With this in mind, A549 cells were incubated with BNG and BN, respectively. As shown in Fig. 4F and G, the turn-on fluorescence signal at 825 nm was found in both BNG and BN groups, suggesting that the acidic tumor microenvironment triggered nanoparticles' dissociation, with BP_5-Cy-B release.

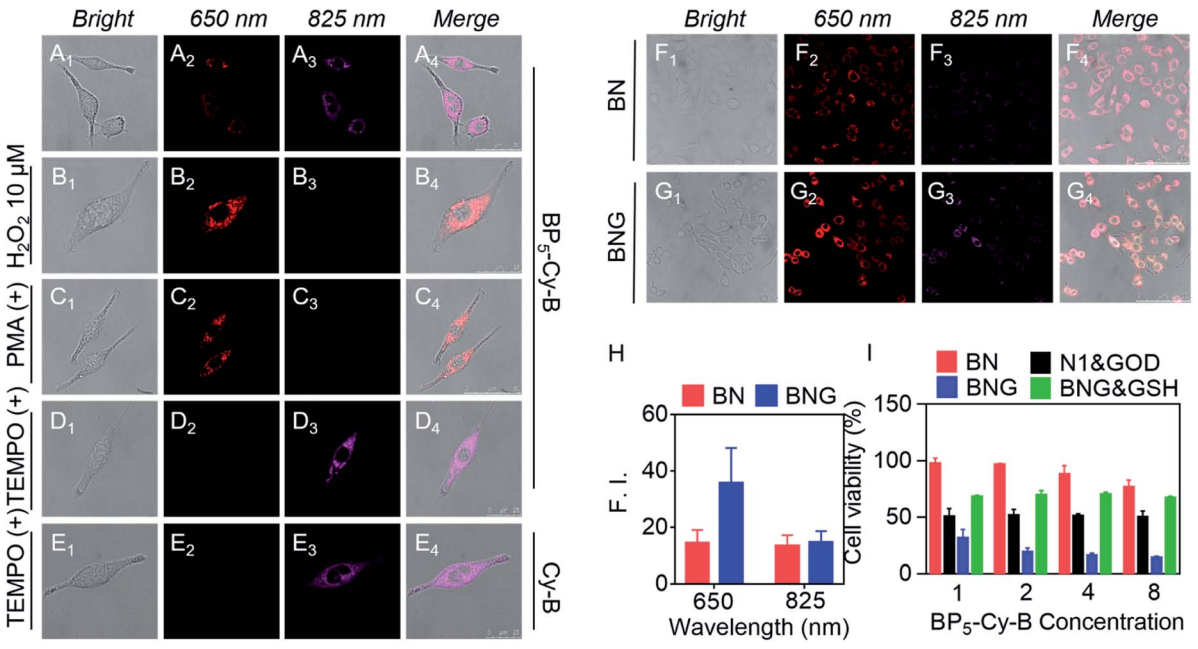

Fig. 4 Dual-channel fluorescence tracking of the cascade process and the effects of BNG in living cells. A549 cancer cells were incubated with (A) BP_5-Cy-B, (B) H_2O_2 and BP_5-Cy-B, (C) PMA and BP_5-Cy-B, (D) TEMPO and BP_5-Cy-B, (E) TEMPO and Cy-B, (F) BN, and (G) BNG. (H) Relative dual-channel NIR fluorescence intensity of A549 cells incubated with BN and BNG; (I) A549 cells with different treatments for 48 h and using a MTT assay to determine the cell viability.

Notably, compared with BN (without GOD), BNG exhibited a much stronger fluorescence signal at 650 nm (Fig. 4H). This different signal intensity at 650 nm between BNG and BN proves that the H_2O_2 level of the BNG group is much higher than that of BN. This difference could be attributed to the role of GOD in BNG, catalyzing the oxidation reaction in cancer cells for the generation of a large amount of H_2O_2. All these living cell imaging results provided solid evidence that the orchestrated nanotheranostic BNG could be activated by the acidic tumor microenvironment and track the release and biocatalytic behavior of GOD in living cells in real time.

In vivo tracking of GOD-based release and its biocatalytic behavior for synergistic therapy

Next, BNG cascade nanotheranostics was further studied for its synergistic cancer treatment. In fact, BP_5-Cy-B and/or N1 exhibited almost no cytotoxic effects on cells with good biocompatibility. In contrast, GOD loaded in the copolymer of N1 displayed enhanced cytotoxicity in cancer cells, suggestive of the oxidative stress resulting from GOD enzymes. Impressively, BNG exhibited significantly enhanced cytotoxicity (with extremely low cell viability of 14.1%) compared to other formulations (Fig. 4I). The remarkable cytotoxicity of BNG could be interpreted from two aspects: (i) the oxidative damage caused by GOD and (ii) MC effectively depleting intracellular GSH, thus weakening the antioxidative capability of the cancer cells (Fig. S8†). Furthermore, the addition of GSH (antioxidant) into the media significantly abolished the inhibition efficiency of BNG, further confirming the great importance of GSH depletion in achieving a synergistic therapeutic performance. These results demonstrate that our cascade nanotheranostics system could realize synergistic cancer treatment.

The above promising results in solution and in living cells inspired us to further explore the feasibility of BNG in living mice. After the intravenous injection of A549 xenograft tumor-bearing mice, the *in vivo* behavior of BNG and BN was tracked by the dual-channel fluorescence read-out signal (yellow-red represented at 825 nm; rainbow represented at 650 nm). As shown in Fig. 5A and C, after injection of BN or BNG for 3 h, we observed that the fluorescence at 825 nm of both groups was turned on and concentrated at the tumor site. This result verified that BNG could be activated by the acidic tumor microenvironment and the GOD enzyme release. Besides, this excellent tumor-targeting phenomenon might be attributed to three reasons: (i) the EPR effect of assembled nanoparticles, (ii) ultrasensitive pH-activated targeting ability from copolymer N1, and (iii) biotin-based active targeting. Meanwhile, very weak fluorescence at 650 nm was observed in the BN group, which could be attributed to the response of BP_5-Cy-B towards the low concentration of endogenous H_2O_2 in the tumor site (Fig. 5B). In contrast, BNG displayed much stronger fluorescence at 650 nm (Fig. 5D), which could be attributed to the biocatalytic behavior of GOD. Furthermore, as shown in Fig. 5B and D, the fluorescence intensity of BNG at 650 nm is still much stronger

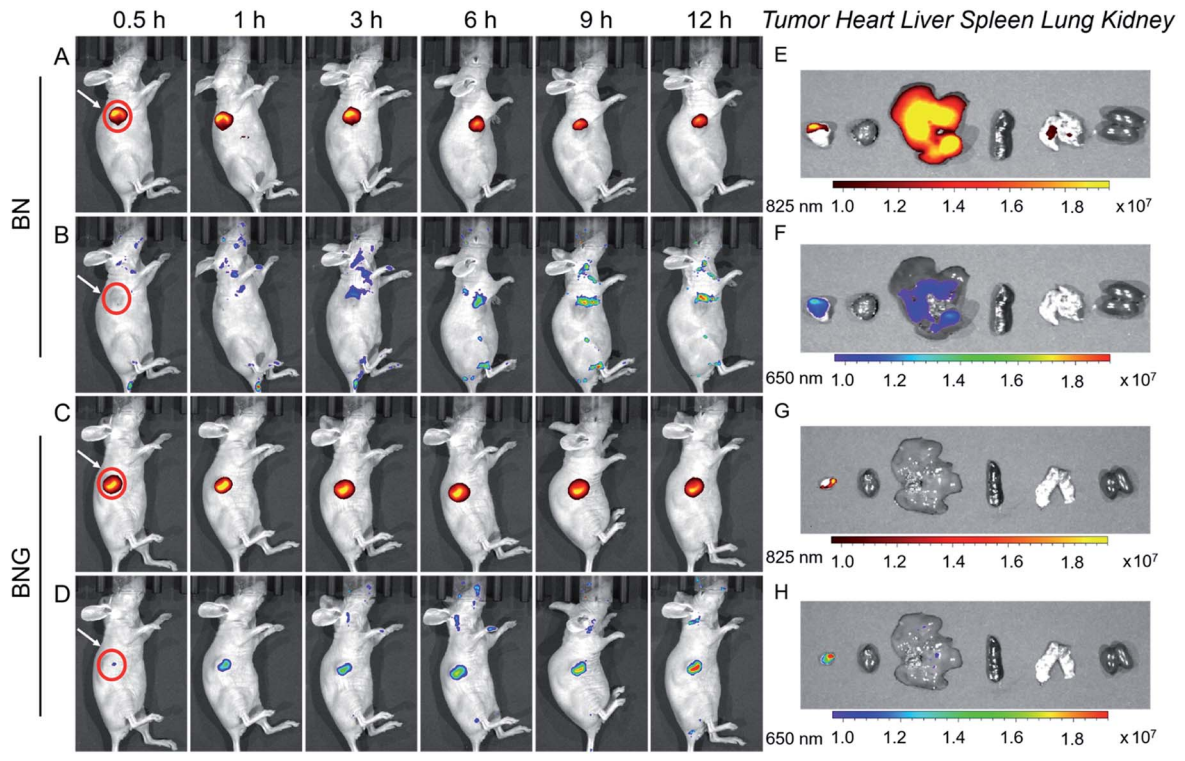

Fig. 5 Dual-channel fluorescence tracking of the GOD-based cascade process *in vivo*. Dual-channel NIR-fluorescence imaging of A549 xenograft tumor-bearing mice at various times (0.5, 1, 3, 6, 9 and 12 h) after the intravenous injection of (A and B) BN and (C and D) BNG, administered at a BP_5-Cy-B-equivalent dose of 0.1 mg kg^{-1}. *Ex vivo* NIR-fluorescence imaging of the excised organs (tumor, heart, liver, spleen, lung, kidney) 12 h after the intravenous injection of (E and F) BN and (G and H) BNG.

than that of BN, which suggests a continuous triggered GOD release by the lower pH values. These results demonstrate that our cascade nanotheranostics could track or visualize the GOD-based cascade process in real time.

After 12 h of intravenous injection, the tumors and major organs were collected to investigate the biodistribution BNG. As shown in Fig. 5G and H, the dual-channel fluorescence of BNG revealed that it mainly distributed in the tumor region, and there was weak fluorescence in the liver and no fluorescence in the other organs (heart, liver, spleen, lung, and kidney). We believe that BNG is inactive in normal tissues and only specifically active in tumor tissues. All of these *in vivo* results show that BNG possesses the striking characteristics of good targeting properties and the real-time visualization of the release of GOD and its *in vivo* cascade process.

Conclusions

In summary, we focused on how to predict and regulate the *in vivo* GOD-based cascade reaction in real time, thus enabling efficient cancer treatment. As proof of concept, we describe a cascade nanotheranostic system (BNG) with GOD enzyme and dual-channel NIR molecular fluorescent probes coloaded in a pH-sensitive copolymer. The cascade reactions, driven by two stimuli, pH and H_2O_2, are monitored by the dual-channel fluorescent signals NIR-1 and NIR-2. The nanoparticles remain silent in the blood circulatory system, but are selectively activated at the tumor site synchronously with *in vivo* turn-on of the NIR-1 channel output and the release of GOD enzyme. Then, the highly efficient generation of H_2O_2 activates BP_5-Cy-B and thus produces MC, which is monitored by the fluorescent signal shift from NIR-1 to NIR-2. During this cascade reaction process, BNG realized effective synergistic therapy as follows: (i) the GOD enzyme-catalyzed oxidation reaction induced increased oxidative stress through intratumoral H_2O_2 generation and (ii) subsequently, the self-destruction of BP_5-Cy-B released MC for GSH depletion. BNG was successfully utilized for strengthening the antitumor therapy, improving the tumor-specific targeting abilities and predicting the therapeutic process. Taken together, the design strategy for BNG represents a feasible approach for promoting the *in vivo* therapeutic application of nanotheranostics, integrating GOD-based synergistic therapy and optical imaging/sensing. We believe this work will open up new horizons for exploring novel designed nanotheranostic strategies for cancer treatment. It is believed that this work not only broadens the applications of GOD-based nanotheranostics but also presents a new visualization strategy for designing effective chemodynamic therapy agents.

Conflicts of interest

There are no conflicts to declare.

Acknowledgements

This work was supported by the NSFC/China (21788102, 21636002, 21622602, 21878087 and 21908060), National Key Research and Development Program (2017YFC0906902 and 2016YFA0200300), the Innovation Program of Shanghai Municipal Education Commission, Shanghai Science and Technology Committee (17520750100), the Shuguang Program (18SG27), and the China Postdoctoral Science Foundation (2019M651417). This study was performed in strict accordance with the NIH guidelines for the care and use of laboratory animals (NIH Publication No. 85-23 Rev. 1985) and was approved by the Institutional Animal Care and Use Committee of National Tissue Engineering Center (Shanghai, China).

Notes and references

1 H. B. Cheng, Y. Li, B. Z. Tang and J. Yoon, *Chem. Soc. Rev.*, 2020, **49**, 21–31.
2 L. C. Murfin, M. Weber, S. J. Park, W. T. Kim, C. M. L. Alled, C. L. McMullin, F. P. Caggiano, C. L. Lyall, G. K. Kohn, J. Wenk, S. D. Bull, J. Yoon, H. M. Kim, T. D. James and S. E. Lewis, *J. Am. Chem. Soc.*, 2019, **141**, 19389–19396.
3 T. Zhang, Y. Li, Z. Zheng, R. Ye, Y. Zhang, R. T. K. Kwok, J. W. Y. Lam and B. Z. Tang, *J. Am. Chem. Soc.*, 2019, **141**, 5612–5616.
4 Z. Yu, W. Pan, N. Li and B. Tang, *Chem. Sci.*, 2016, **7**, 4237–4244.
5 F. Hu, G. Qi, K. Kenry, D. Mao, S. Zhou, M. Wu, W. Wu and B. Liu, *Angew. Chem., Int. Ed.*, 2019, **58**, 1–6.
6 H. Li, W. Shi, X. Li, Y. Hu, Y. Fang and H. Ma, *J. Am. Chem. Soc.*, 2019, **141**, 18301–18307.
7 J. Peng, A. Samanta, X. Zeng, S. Han, L. Wang, D. Su, D. T. Loong, N. Y. Kang, S. J. Park, A. H. All, W. Jiang, L. Yuan, X. Liu and Y. T. Chang, *Angew. Chem., Int. Ed.*, 2017, **56**, 4165–4169.
8 N. K. Lifshin, E. Segal, L. Omer, M. Portnoy, R. S. Fainaro and D. Shabat, *J. Am. Chem. Soc.*, 2011, **133**, 10960–10965.
9 C. Yik-Sham Chung, G. A. Timblin, K. Saijo and C. J. Chang, *J. Am. Chem. Soc.*, 2018, **140**, 6109–6121.
10 Z. Yu, P. Zhou, W. Pan, N. Li and B. Tang, *Nat. Commun.*, 2018, **9**, 5044.
11 H. Cheng, X. Y. Jiang, R. R. Zheng, S. J. Zuo, L. P. Zhao, G. L. Fan, B. R. Xie, X. Y. Yu, S. Y. Li and X. Z. Zhang, *Biomaterials*, 2019, **195**, 75–85.
12 L. H. Fu, C. Qi, Y. R. Hu, J. Lin and P. Huang, *Adv. Mater.*, 2019, **31**, 1808325.
13 M. H. Lee, A. Sharma, M. J. Chang, J. Lee, S. Son, J. L. Sessler, C. Kang and J. S. Kim, *Chem. Soc. Rev.*, 2018, **47**, 28–52.
14 Q. Qi, W. Chi, Y. Li, Q. Qiao, J. Chen, L. Miao, Y. Zhang, J. Li, W. Ji, T. Xu, X. Liu, J. Yoon and Z. Xu, *Chem. Sci.*, 2019, **10**, 4914–4922.
15 C. Liu, J. Xing, O. U. Akakuru, L. Luo, S. Sun, R. Zou, Z. Yu, Q. Fang and A. Wu, *Nano Lett.*, 2019, **19**, 5674–5682.
16 P. Cui, D. P. McMahon, P. R. Spackman, B. M. Alston, M. A. Little, G. M. Day and A. I. Cooper, *Chem. Sci.*, 2019, **10**, 9988–9997.
17 A. B. Aletti, S. Blasco, S. J. Aramballi, P. E. Kruger and T. Gunnlaugsson, *Chem*, 2019, **5**, 2617–2629.
18 Z. Xue, E. Zhang, J. Liu, J. Han and S. Han, *Angew. Chem., Int. Ed.*, 2018, **57**, 10096–10101.

19 G. Feng, J. Wang, M. Boronat, Y. Li, J. H. Su, J. Huang, Y. Ma and J. Yu, *J. Am. Chem. Soc.*, 2018, **140**, 4770–4773.
20 W. Ke, J. Li, F. Mohammed, Y. Wang, K. Tou, X. Liu, P. Wen, H. Kinoh, Y. Anraku, H. Chen, K. Kataoka and Z. Ge, *ACS Nano*, 2019, **13**, 2357–2369.
21 Z. Xu, X. Huang, X. Han, D. Wu, B. Zhang, Y. Tan, M. Cao, S. H. Liu, J. Yin and J. Yoon, *Chem*, 2018, **4**, 1609–1628.
22 K. Umezawa, M. Kamiya and Y. Urano, *Angew. Chem., Int. Ed.*, 2018, **57**, 9346–9350.
23 F. Yu, P. Li, B. Wang and K. Han, *J. Am. Chem. Soc.*, 2013, **135**, 7674–7680.
24 X. Han, X. Song, F. Yu and L. Chen, *Chem. Sci.*, 2017, **8**, 6991–7002.
25 C. Yan, Z. Guo, Y. Liu, P. Shi, H. Tian and W. H. Zhu, *Chem. Sci.*, 2018, **9**, 6176–6182.
26 H. Fan, G. Yan, Z. Zhao, X. Hu, W. Zhang, H. Liu, X. Fu, T. Fu, X. B. Zhang and W. Tan, *Angew. Chem., Int. Ed.*, 2016, **55**, 5477–5482.
27 J. Li, A. Dirisala, Z. Ge, Y. Wang, W. Yin, W. Ke, K. Toh, J. Xie, Y. Matsumoto, Y. Anraku, K. Osada and K. Kataoka, *Angew. Chem., Int. Ed.*, 2017, **56**, 14025–14030.
28 A. Sharma, M. G. Lee, M. Won, S. Koo, J. F. Arambula, J. L. Sessler, S. G. Chi and J. S. Kim, *J. Am. Chem. Soc.*, 2019, **141**, 15611–15618.
29 X. Wan, H. Zhong, W. Pan, Y. Li, Y. Chen, N. Li and B. Tang, *Angew. Chem., Int. Ed.*, 2019, **58**, 14134–14139.
30 Y. Yang, Y. Lu, P. L. Abbaraju, I. Azimi, C. Lei, J. Tang, M. Jambhrunkar, J. Fu, M. Zhang, Y. Liu, C. Liu and C. Yu, *Adv. Funct. Mater.*, 2018, **28**, 1800706.
31 S. Wang, Z. Wang, G. Yu, Z. Zhou, O. Jacobson, Y. Liu, Y. Ma, F. Zhang, Z. Y. Chen and X. Chen, *Adv. Sci.*, 2019, **6**, 1801986.
32 T. Gu, Y. Wang, Y. Lu, L. Cheng, L. Feng, H. Zhang, X. Li, G. Han and Z. Liu, *Adv. Mater.*, 2019, **31**, 1806803.
33 X. Zhao, C. X. Yang, L. G. Chen and X. P. Yan, *Nat. Commun.*, 2017, **8**, 14998.
34 B. Yang, Y. Chen and J. Shi, *Adv. Mater.*, 2019, **31**, 1901778.
35 Y. Wu, J. Chen, L. Sun, F. Zeng and S. Wu, *Adv. Funct. Mater.*, 2019, **29**, 1807960.
36 Z. Wang, H. Wu, P. Liu, F. Zeng and S. Wu, *Biomaterials*, 2017, **139**, 139–150.
37 M. Huo, L. Wang, Y. Chen and J. Shi, *Nat. Commun.*, 2017, **8**, 357.
38 M. Ye, Y. Han, J. Tang, Y. Piao, X. Liu, Z. Zhou, J. Gao, J. Rao and Y. Shen, *Adv. Mater.*, 2017, **29**, 1702342.
39 B. Yang, Y. Chen and J. Shi, *Chem. Rev.*, 2019, **119**, 4881–4985.
40 Z. Zheng, T. Zhang, H. Liu, Y. Chen, R. T. K. Kwok, C. Ma, P. Zhang, H. H. Y. Sung, I. D. Williams, J. W. Y. Lam, K. S. Wong and B. Z. Tang, *ACS Nano*, 2018, **12**, 8145–8159.
41 Y. Liu, M. Chen, T. Cao, Y. Sun, C. Li, Q. Liu, T. Yang, L. Yao, W. Feng and F. Li, *J. Am. Chem. Soc.*, 2013, **135**, 9869–9876.
42 T. Ma, Y. Hou, J. Zeng, C. Liu, P. Zhang, L. Jing, D. Shangguan and M. Gao, *J. Am. Chem. Soc.*, 2018, **140**, 211–218.
43 H. Guo, G. Chen, M. Gao, R. Wang, Y. Liu and F. Yu, *Anal. Chem.*, 2019, **91**, 1203–1210.
44 Z. Guo, Y. Ma, Y. Liu, C. Yan, P. Shi, H. Tian and W. H. Zhu, *Sci. China: Chem.*, 2018, **61**, 1293–1300.
45 W. Sun, S. Guo, C. Hu, J. Fan and X. Peng, *Chem. Rev.*, 2016, **116**, 7768–7817.
46 T. B. Ren, Q. L. Zhang, D. Su, X. X. Zhang, L. Yuan and X. B. Zhang, *Chem. Sci.*, 2018, **9**, 5461–5466.
47 M. Tian, J. Sun, B. Dong and W. Lin, *Angew. Chem., Int. Ed.*, 2018, **57**, 16506–16510.